ELSEVIER

Synthetic Metals 84 (1997) 709-714

SYNTHETIC METALS

Inhomogeneous Insulator-Metal Transition in Conducting Polymers

R. S. Kohlman[a], D. B. Tanner[b], G. G. Ihas[b], Y. G. Min[c], A. G. MacDiarmid[c], and A. J. Epstein[d]
[a] Department of Physics, The Ohio State University, Columbus, Ohio 43210-1106, USA
[b] Department of Physics, University of Florida, Gainesville, Florida 32611-8440, USA
[c] Department of Chemistry, University of Pennsylvania, Philadelphia, Pennsylvania, 19104-6323, USA
[d] Department of Physics and Department of Chemistry, The Ohio State University, Columbus, Ohio 43210-1106, USA

Abstract

A review of recent work on the insulator-metal transition (IMT) in conducting polymers is presented. The temperature dependence of the dielectric function [$\varepsilon(\omega)$] of highly conducting polyaniline and polypyrrole, which cross the IMT as probed by $\sigma_{DC}(T)$, has been measured over an unusually broad range of frequencies (6.5 GHz and 2 meV - 6 eV). These data demonstrate that the inhomogeneous disorder model is a more appropriate description for the IMT than the homogeneous three-dimensional Anderson model.

Keywords: Metal-insulator transitions, Polyaniline, Polypyrrole, Dielectric function, Reflection spectroscopy, Transport measurements

1. Introduction

Extensive research over the past two decades has focused on the metallic state in conducting polymers. For most conducting polymers, a high dc conductivity (σ_{DC}) at room temperature (*RT*) is coupled with a strong *T* dependence due to structural disorder, resulting in insulating behavior at low *T* [1,2]. However, over the last decade, conducting polyacetylene [$(CH)_x$] [3], polypyrrole (PPy) [3], and polyaniline (PAN) [4,5] have been reported with finite metallic σ_{DC} down to millikelvin (mK) *T*. Accompanied by a finite density of states at the Fermi level [$N(E_F)$] [1,2] and other metallic signatures [1,2] it is clear experimentally that an insulator-metal transition (IMT) has occurred and a metallic state exists in selected conducting polymers.

The IMT in these inhomogeneously disordered networks of quasi-1D chains has been described by both inhomogeneous disorder models [1,2,6-11] and the homogeneous three-dimensional (3D) Anderson model [12,13]. The conducting polymers PAN and PPy, with $\sigma_{DC}(RT)$ close to the minimum metallic conductivity ($\sigma_{min} \sim 0.03e^2/\hbar a \sim 100$ S/cm [14-16]), are ideal anisotropic systems to study whether the IMT in conducting polymers is due to a homogeneous 3D Anderson transition or percolation on an inhomogeneously disordered network.

A 3D Anderson transition occurs in the presence of large randomly distributed (uniform) disorder. A mobility edge (E_C) separates localized from extended states [14-17] and the scattering time (τ) varies slowly with energy in the vicinity of E_C [18]. At the IMT, the electronic localization length diverges. A monotonic evolution of the transport properties is predicted as E_F crosses E_C into the region of delocalized states [14]. In particular, σ_{DC} grows in magnitude, as its *T* dependence weakens [14] and the slope of the logarithmic derivative of σ_{DC} ($W = d ln\sigma_{DC}(T)/d lnT$) [19] changes sign from negative to positive. Because of the large disorder required to localize electronic wavefunctions in 3D, the Ioffe-Regel condition [20] requires $k_F\lambda \sim 1$, where k_F is the Fermi wavevector and λ is the mean free path, resulting in the slowly varying τ being short (typically $\sim 10^{-15}$ s). For short τ, localization corrections to the metallic Drude response result in a dielectric function [$\varepsilon(\omega)$] that is positive at low energy [13,15,16,18] even on the metallic side of the IMT, in contrast to the large negative low energy $\varepsilon_{Drude}(\omega)$ for usual metals [21]. τ will decrease at low *T* due to thermal depopulation of more extended states.

In contrast, a very different IMT is presented by an array of 3D (spatially [22,23] and electronically [24] anisotropic) metallic ellipsoids with an open Fermi surface [1,7-9] separated by a disordered quasi one-dimensional (Q-1D) medium (Inhomogeneous Disorder Model). Conduction electrons in isolated 1D systems are readily localized by even small disorder [14] with the localization length increasing as the disorder decreases. When the localization length in the quasi 1D disordered regions exceeds the separation between metallic ellipsoids for a sufficient fraction of the sample, an IMT occurs [8,25]. As for a 3D Anderson transition, there is a crossover in sign of the low *T* slope of *W* as the IMT is achieved, though the IMT is not necessarily a monotonic function of $\sigma_{DC}(RT)$. The low frequency transport in this case is dominated by a fraction of the carriers (δ) which percolate through the network [26]. $\sigma_{DC}(T)$ for the network may show a metallic *T* dependence near *RT* if the disorder is weak enough even though localization dominates at lower *T* [8]. Due to the open Fermi surface of the anisotropic polymer metal, a very long τ may be associated with the fraction δ of carriers present at percolation. For this circumstance at 0 K, $\varepsilon(\omega)$ will become negative below a screened plasma frequency $\Omega_p/\varepsilon_b^{1/2}$ [21] [$\Omega_p = (4\pi\delta ne^2/m^*)^{1/2}$ where *n* is the full carrier density and m^* is the effective mass of the fraction δ of delocalized carriers and ε_b is the limiting value of the dielectric function for bound carriers] and increase to large negative values for $\omega \ll \Omega_p/\varepsilon_b^{1/2}$. Due to phonon induced delocalization in the quasi-1D disordered regions, $\varepsilon(\omega)$ can have this behavior at finite *T even for samples on the insulator side of the IMT at 0 K*. $\tau(T)$ will depend upon the distribution of percolated paths and importance of phonon-induced delocalization.

PII S0379-6779(96)04115-X

Because of the distinctions between a 3D Anderson IMT and an inhomogeneous disorder IMT at low frequency, systematic probes of the electronic response away from E_F effectively distinguish between these models. In this paper, we review the temperature dependence and frequency response over an unusually broad range of optical frequencies (2 meV - 6 eV) and at microwave frequencies (6.5 GHz) of $\varepsilon(\omega)$ for samples of conducting PAN and PPy that cross the IMT as probed by $\sigma_{DC}(T)$ (down to ~20 mK for selected samples). These data demonstrate that the IMT is due to inhomogeneous disorder and not a homogeneous 3D Anderson transition. In particular, as $\sigma_{DC}(RT)$ increases, the T dependence of σ_{DC} does not weaken monotonically so that some samples with $\sigma_{DC}(RT) > \sigma_{min}$ become insulating at low T. Also, the mK σ_{DC} demonstrate a nonmonotonic T dependence and a negative magnetoresistance inconsistent with variable range hopping expected for insulating samples within an Anderson IMT. $\varepsilon(\omega)$ shows free carrier (Drude) dispersion in the far infrared (IR) for PAN samples with $\sigma_{DC}(RT) >$ ~100 S/cm and associated very long τ of > 10^{-13} s, much longer than the Ioffe-Regel condition allows. As T decreases, τ increases, inconsistent with the expectations of thermal occupancy in the Anderson model. However, only a small fraction (10^{-3}) of the carriers [those which dominate $\sigma_{DC}(T)$] are delocalized with these long τs. Also, as the low T $W(T)$ plot crosses from negative slope (insulating) to positive slope (conducting) for different samples, the RT Ω_p does not increase monotonically, inconsistent with expectations of the Anderson model.

2. Experimental

The PAN films were doped with d,1-camphorsulfonic acid (H^+CSA^-). Samples C and D were prepared by mixing emeraldine base (EB) and HCSA separately in *m*-cresol before mixing the solutions, doping them in solution. The remaining films were prepared by grinding stoichiometric amounts of EB and HCSA powders with mortar and pestle before dissolution in a mixture of *m*-cresol and chloroform. Sample A and B were cast from *m*-cresol [23,27] while E was cast from a 30%/70% mixture of *m*-cresol/chloroform [23]. The conducting PPy was doped electrochemically [3] with hexafluorophosphate (PF_6). The detailed techniques for measuring $\sigma_{DC}(T)$ (4.2 - 300 K) and $\varepsilon_{MW}(T)$ were reported previously [7]. The mK σ_{DC} was measured by mounting the samples on the mixing chamber of a ^{3}He-^{4}He dilution refrigerator and applying the four probe technique, using a low frequency (19 Hz) signal [4,5]. A magnetic field was applied normal to the transport direction. The T dependent reflectance [$R(T)$] (50-10,000 cm^{-1}) was measured using a BOMEM DA3 FTIR spectrometer equipped with a continuous flow He cryostat. The far IR (10-100 cm^{-1}) $R(T)$ was measured using a Michelson interferometer [4] equipped with a continuous flow He cryostat. The high energy (5,000-50,000 cm^{-1}) reflectance was measured at RT using a Perkin Elmer Lambda 19 UV/VIS spectrometer equipped with an integrating sphere. The optical dielectric functions [$\varepsilon(\omega)$] were calculated via a Kramers- Kronig (KK) analysis [9,10,21]. The extrapolations used in the KK analysis were described previously [9].

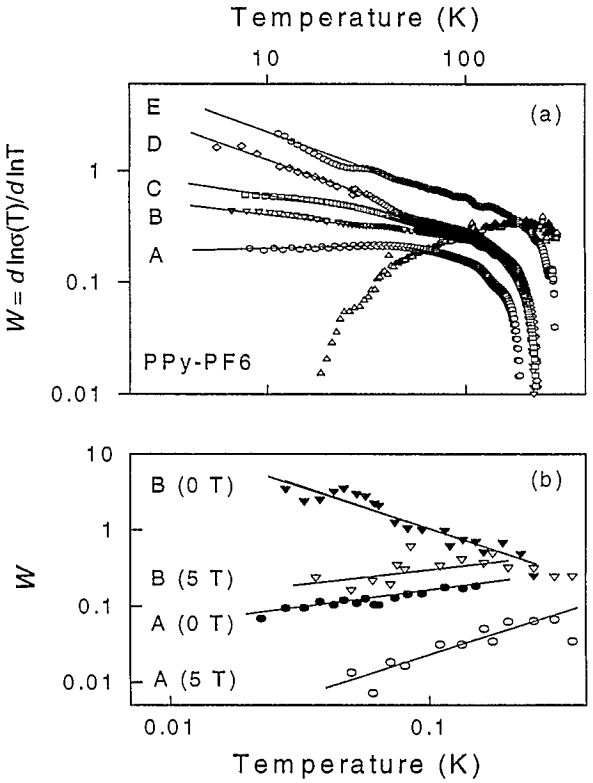

Figure 1. Reduced activation energy [W = $d ln\sigma_{DC}(T)/d lnT$].(a) from 4-300 K for PPy-PF_6 and PAN-CSA samples and (b) from 20 mK- 0.3 K for PAN-CSA samples A and B with and without 5 Tesla magnetic field.

3. Results and Discussion

A material on the metallic side of the IMT will demonstrate a positive slope at low T for the logarithmic temperature derivative of σ_{DC} [W = $d ln\sigma_{DC}(T)/d lnT$] [19] and a finite σ_{DC} as T → 0 [14]. The plot of log$W$ versus log$T$ is shown in Fig. 1(a) in the absence of a magnetic field. For hopping (insulating) transport [$\sigma_{DC}(T) = \sigma_0 exp[-(T_0/T)^{\alpha}]$] [12,14,15,19], log$W$ = constant - αlog$T$; therefore the plot of log$W$ vs log$T$ will have a negative slope at low T. W has a negative slope for PAN-CSA samples B-E and α increases from 0.3-0.6 for those samples, indicative of hopping behavior. In contrast, log$W$ for PPy-PF_6 and PAN-CSA sample A have a positive slope, characteristic of metallic behavior [19]. For PAN-CSA (A), the W plot possesses a positive slope down to ~20 mK, Fig. 1(b). When a magnetic field (H) of 5 Tesla is applied, the positive slope of the W plot becomes greater, indicating that H induces a more metallic state. An applied magnetic field *actually induces a crossover in the mK W plot for PAN-CSA sample B from insulating (slope ~-1) to metallic*, suggesting the importance of weak localization [15,16] and percolation phenomena [28].

$\sigma_{DC}(T)$ for PPy-PF_6 and PAN-CSA samples A-E is shown in Fig. 2 down to 20 mK for selected samples. Both PPy-PF_6 and PAN-CSA sample A with metallic W plots have a large finite σ_{DC}

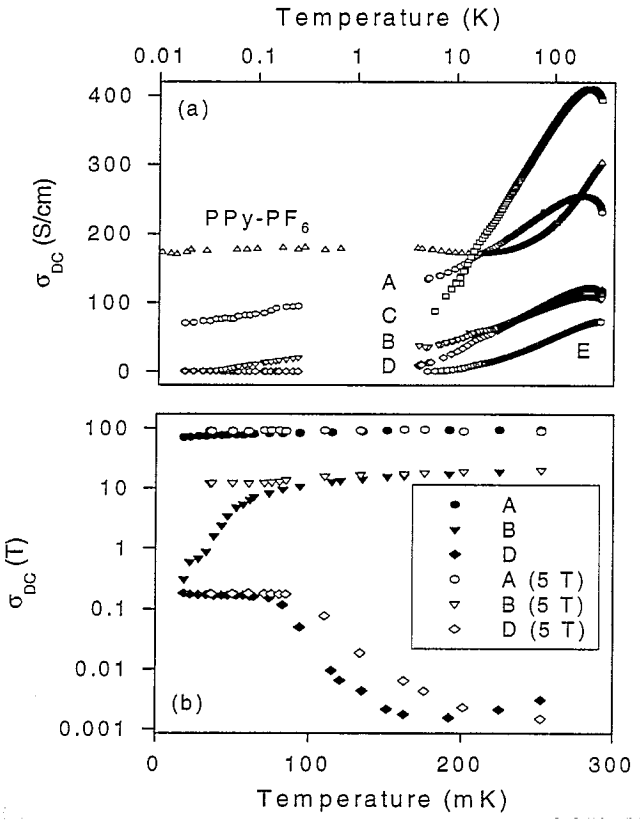

Figure 2. (a) $\sigma_{DC}(T)$ for PPy-PF_6 from Ref. [3] and PAN-CSA from RT down to 20 mK for selected samples. (b) mK σ_{DC} and magnetoconductance for selected PAN-CSA samples.

(> 170 S/cm [3] and 70 S/cm respectively) down to ~20 mK. For the remaining samples, σ_{DC} becomes small at low T, consistent with the insulating character of their W plots. The mK $\sigma_{DC}(T)$ for PAN- CSA sample D has a minimum at ~0.18 K, below which it increases and saturates, similar to the T dependence seen in PPy-PF_6 below ~20 K [3,9]. This T dependence is different from the monotonic behavior associated with variable range hopping [14-16]. It is reminiscent of charge motion in narrow band systems such as for small polarons [29]. We speculate that it may be associated with metallic electrons transiting disordered polymer regions where k_BT is less than a narrow bandwidth. The large difference in the T at which this behavior occurs for PAN-CSA and PPy-PF_6 may be due to the different local order in these systems [22]. Also, the PPy disordered regions likely have larger bandwidths due to fewer atoms per repeat and negligible steric interactions among adjacent repeat units which introduce band narrowing ring twists. Application of a magnetic field results in a negative magnetoresistance (*MR*) for each of the materials. A negative *MR* is consistent with both destruction of weak quantum localization by H [15,16] and enhanced delocalization on a percolating network [28]. A negative *MR* has also been reported for highly conducting PPy-PF_6 [3,5] and doped $(CH)_x$ [1-3,30].

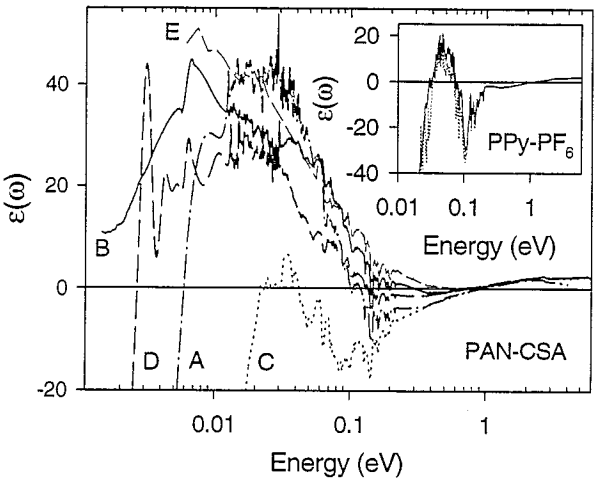

Figure 3. *RT* $\varepsilon(\omega)$ for PAN-CSA samples. Inset, $\varepsilon(\omega)$ for PPy-PF_6 shown at RT (solid line) and 10 K (dotted line).

Near *RT* for the PAN-CSA samples A-D, σ_{DC} increases with decreasing T (metallic behavior), reaches a maximum, and then decreases at low T. This $\sigma_{DC}(T)$ is consistent with the predictions of the inhomogeneous disorder model [8]. The maximum in $\sigma_{DC}(T)$ is likely absent in PPy-PF_6 due to greater disorder [22]. Even though PAN-CSA (A) is metallic at low T, insulating PAN-CSA (C) has the highest $\sigma_{DC}(RT)$ ($> \sigma_{min}$); however, C becomes insulating at low T. Similar crossover behavior in $\sigma_{DC}(T)$ occurs for PAN-CSA samples B and D. Thus the T dependence of σ_{DC} does not monotonically become weaker (more metallic) with increasing $\sigma_{DC}(RT)$ as expected for an IMT in the homogeneous 3D Anderson model [14]. For PAN-CSA sample E, σ_{DC} decreases monotonically with decreasing T, indicating stronger localization.

Figure 3 shows the *RT* $\varepsilon(\omega)$ for PPy-PF_6 [9] and for the PAN-CSA samples [10] which cross the IMT. As the PAN-CSA samples approach the IMT from the insulating side, $\varepsilon(\omega)$ shows two different behaviors. For PAN-CSA samples A-E, a zero crossing of $\varepsilon(\omega)$ develops at ~1 eV, the screened plasma frequency ω_{p1} [$= \Omega_{p1}/\varepsilon_b^{1/2}$, where $\Omega_{p1} = (4\pi ne^2/m_1^*)^{1/2}$, m_1^* is an averaged effective mass of the carriers and ε_b is the background dielectric function]. However, $\varepsilon(\omega)$ becomes positive in the far IR after a second zero crossing due to strong disorder scattering (localization) [13-16,18]. PAN-CSA sample E demonstrates localized behavior with $\varepsilon(\omega)$ positive in the far IR. Drude formula fits from ~0.4 - 2 eV for samples A-E [4] indicate that the scattering time for these localized carriers is small, $\tau_1 \sim 10^{-15}$ s, consistent with the Ioffe-Regel criterion [20] for localized carriers. Also, Ω_{p1} ~2 eV, as expected for full doping in both PAN [23] and PPy [3].

For PPy-PF_6, metallic PAN-CSA sample A, and insulating PAN-CSA samples C-D, (and likely for insulating sample B), $\varepsilon(\omega)$ has three zero crossings, Fig. 3. The lowest frequency crossing occurs at the screened plasma frequency ω_p [$= \Omega_p/\varepsilon_b^{1/2}$], Table I, in

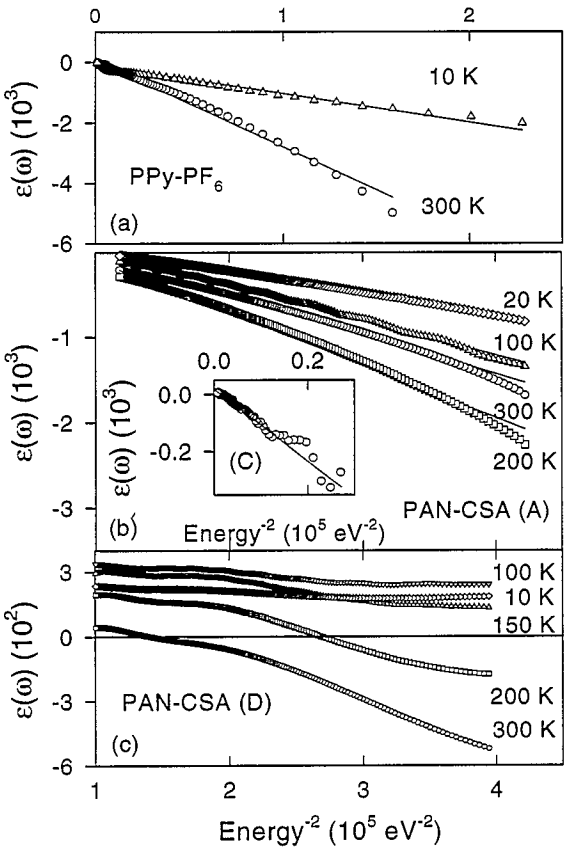

Figure 4. ε(ω) versus $1/\omega^2$ at different T for (a) PPy-PF_6, (b) PAN-CSA sample A, Inset PAN-CSA sample C at *RT*, and (c) PAN-CSA sample D.

the far IR (< ~0.03 eV), below which ε(ω) remains negative as expected for free carriers [21]. Similarly, there are signatures of a low frequency ω_p for highly conducting doped $(CH)_x$ [31]. The inset to Fig. 3 shows the 10 K ε(ω) (10-10,000 cm^{-1}) for PPy-PF_6. There is negligible T dependence in the vicinity of ω_{p1}, indicating that these carriers are strongly localized by disorder, likely contributing < 10 S/cm to the total *RT* σ_{DC} (based on $\sigma_{DC}(RT)$ of disordered samples [1,2]). A similar lack of T dependence was reported for ω_{p1} in PAN-CSA samples [13]. In contrast, the far IR (< 0.1 eV) ε(ω) for PPy-PF_6 and PAN-CSA samples A and D, Fig. 4, show a T dependence, suggesting that the carriers which give rise to ω_p are responsible for the low frequency and dc metallic transport. For metallic PPy-PF_6 and PAN-CSA sample A, ε(ω) remains negative in the far IR down to low T (~10 K), indicating that free carriers are present at low T in the metallic samples. In contrast, ε(ω) for insulating PAN-CSA (D) crosses from negative to positive in the far IR as T decreases, indicating that the free carriers become localized at low T (perhaps forming a "pinned mode" at higher frequencies) for samples on the insulating side of the IMT. For insulating PAN-CSA (D), the loss of free carriers occurs concomitant with the rapid drop in σ_{DC} at low T.

Since ε(ω) does not saturate down to the lowest measured frequencies for PPy-PF_6, PAN-CSA samples A, C (*RT*), and D (T > 150 K), the Drude model for free carriers with $\tau \gg 1/\omega$ [21]

$$\varepsilon(\omega) = \varepsilon_b - \Omega_p^2/\omega^2, \quad (1)$$

is applicable and therefore for the free carriers, τ > ~1/(0.006 eV) ~ 10^{-13} s. The slope of ε(ω) versus $1/\omega^2$ at various T, Fig. 4, yields the $\Omega_p(T)$ provided in Table I. For both PPy-PF_6 and the PAN-CSA samples, Ω_p ~ 0.1 eV, a small value compared to the full carrier plasma frequency Ω_{p1} ~2 eV. The fraction (δ) of carriers which have large values of τ (> 10^{-13} s) can be estimated, assuming that $m^* \approx m_1^*$, as

$$\delta = (m^*/m_1^*)(\Omega_p/\Omega_{p1})^2 \sim 10^{-3}. \quad (2)$$

It is noted that m^* may be much larger than m_1^* due to band narrowing in the disordered regions. This small δ resembles the case for metal/insulator composites close to the metallic percolation threshold [26].

In addition, $\Omega_p(T)$ scales roughly with $\sigma_{DC}(T)$ [4] and not the low temperature W plot. Therefore, the Ω_p of sample C, for which the 0 K E_F lies in the region of localized states is larger at *RT* than the Ω_p of sample A, for which the 0 K E_F lies in the region of extended (Drude) states. This is in direct contradiction with 3D Anderson model predictions but is in accord with expectations of the inhomogeneous disorder model. For both PPy and PAN, Ω_p decreases at the lowest T. For PAN-CSA (D), ε(ω) shows Drude dispersion only for T > ~150 K in the optical frequency range. At T ~150 K, ε(ω) is positive throughout the far IR, indicating that $\Omega_p \to 0$ (no percolation) at low T for the insulating samples.

By comparing $\Omega_p(T)$ with $\sigma_{DC}(T)$ for PPy-PF_6 and PAN-CSA samples A, C, and D and using the Drude expression:

$$\sigma_{DC}(T) = \Omega_p^2(T)\tau(T)/4\pi, \quad (3)$$

$\tau(T)$ is estimated, Table I. In each case, $\tau \sim 10^{-13}$ s, similar to the τ reported for conducting polyacetylene [31]. This estimate of τ agrees with the estimate $\tau > 1/\omega \sim 10^{-13}$ s made because of the lack of saturation of ε(ω) at low frequency. The agreement of these estimates implies that the metallic σ_{DC} is due to only the delocalized carriers which percolate through the network. This long τ is much greater than allowed by the Ioffe-Regel condition [20]. Since τ varies slowly with energy for 3D Anderson localization, even thermal population of states above E_c is not expected to lead to large τ. On the other hand, phonon-induced delocalization in the quasi-1D disordered regions will lead to a large τ consistent with the inhomogeneous disorder model. For both PPy-PF_6 and PAN-CSA (A), τ is larger at low T than at *RT*. Even for PAN-CSA (D), τ(200 K) > $\tau(RT)$. Therefore, the IMT does not result from an Anderson IMT for which τ decreases at low T due to thermal depopulation of more extended states above E_C. Instead, the IMT is associated with $\Omega_p \to 0$ as $T \to 0$.

Table I

Sample	Temp. (K)	σ_{DC} (S/cm)	ω_p (eV)	Ω_p (eV)	τ (10^{-13} s)	$\Omega_{p,MW}$ (eV)	τ_{MW} (10^{-11} s)
PAN-CSA (A)	300	230	0.006	0.07	2.5	0.007	2.5
	200	250	0.006	0.08	2.0	-	-
	100	240	0.005	0.06	2.9	-	-
	20	170	0.003	0.05	3.4	-	-
PAN-CSA (C)	300	390	0.02	0.11	1.6	0.016	1.1
PAN-CSA (D)	300	120	0.003	0.04	3.7	0.005	2.4
	200	120	0.002	0.03	6.6	-	-
PPy-PF_6	300	300	0.03	0.17	0.5	0.007	3
	10	170	0.03	0.1	0.9	-	-

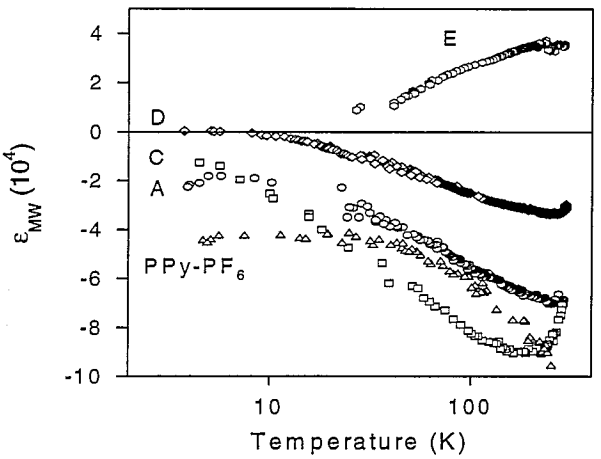

Figure 5. ε_{MW} measured at 6.5 GHz for PPy-PF_6 and selected PAN-CSA samples.

Figure 5 shows the behavior of the microwave (6.5 GHz) dielectric constant (ε_{MW}) with decreasing *T*. For sample E, ε_{MW} is positive at *RT*, consistent with the optical result. For the remaining samples, ε_{MW} is negative at *RT*, confirming the Drude response at optical frequencies. In addition, for PPy-PF_6 and PAN-CSA (A), ε_{MW} remains negative down to ~4 K, providing independent confirmation of free electrons at low *T* in the metallic systems. For insulating PAN-CSA sample C, ε_{MW} remains negative down to ~4 K though showing a much stronger *T* dependence. In contrast, ε_{MW} for PAN-CSA (D) decreases in magnitude down to ~10 K, where it crosses from negative to positive. This confirms the crossover behavior observed in the far IR $\varepsilon(\omega)$ with decreasing *T*. The crossover of $\varepsilon(\omega)$ at optical frequencies occurs at ~150 K while ε_{MW} crosses over at ~10 K, consistent with a continuous shift of ω_p to lower energy as *T* decreases.

In the limit $\omega\tau \ll 1$, the Drude model takes the form:

$$\sigma_{MW} \sim \Omega_{p,MW}^2\tau_{MW}/4\pi, \qquad (4)$$
$$\varepsilon_{MW} \sim \varepsilon_b - \Omega_{p,MW}^2\tau_{MW}^2,$$

where the subscripts *MW* are used to discriminate between the value of Ω_p and τ estimated from the far IR $\varepsilon(\omega)$. The $\Omega_{p,MW}$ and τ_{MW} estimated at *RT* from ε_{MW} and σ_{MW} [4] using the low frequency Drude model are shown in Table I. The $\Omega_{p,MW}$ are generally smaller than the Ω_p estimated from the far IR $\varepsilon(\omega)$ by a factor of 10^1 and the τ_{MW} are larger than τ estimated from $\varepsilon(\omega)$ by a factor of 10^2. The discrepancy between Ω_p and $\Omega_{p,MW}$ and τ and τ_{MW} is attributed to the distribution of scattering times which accompanies an inhomogeneously disordered material. Therefore, Ω_p is a consequence of free carriers with a distribution of τ. In the IR where $\omega \gg 1/\tau$, $\varepsilon(\omega)$ is dominated by the majority of free carriers with shorter τ (~10^{-13} s). At 6.5 GHz, $\varepsilon(\omega)$ has saturated ($\omega\tau \ll 1$) so that it is dominated by a minority of free carriers with the longest τ (~10^{-11} s). We suggest that as *T* decreases, the free carriers with the shortest τ (~10^{-13} s) become localized so that the measured τ increases, reflecting the minority of carriers with longer τ. Due to localization effects, the Drude formula (4) becomes inapplicable at microwave frequencies at low T [18]. Therefore, the low *T* $\Omega_{p,MW}$ and τ_{MW} are not calculated in Table I.

Estimating the Fermi velocity as v_F ~5×10^7 cm/s using a fit of $\sigma(\omega)$ to a localization corrected Drude model [14-16] (consistent with $v_F \sim \hbar k_F/m_e \sim 2 \times 10^7$ cm/s, where $k_F = \pi/2c$ since E_F lies in the center of a polaron band [32] and c = 10.2 Å [22]), $\lambda = v_F\tau \sim 10^3$-$10^5$ Å for the free electrons. A larger m* will, of course, reduce this estimate of λ. This λ is much larger than the crystalline domain size for both PPy-PF_6 (~20 Å [22]) and PAN-CSA (~40 Å [7,22]), indicating that the small fraction (δ) of free carriers diffuse among many crystalline regions, consistent with percolation. For metallic PPy-PF_6 and PAN-CSA (A) with large finite σ_{DC} down to mK *T*, the percolated free carriers are present down to low *T* as gauged by $\varepsilon(\omega)$ and ε_{MW}. For conducting polymers, the percolation is unique because individual polymer chains can be part of both ordered metallic ellipsoids and disordered quasi-1D regions where localization effects are stronger. For PAN-CSA samples B-D, Ω_p is observed at *RT* even though they become insulating at low *T*. This is attributed to the importance of phonon-induced delocalization within the disordered regions [1,4,8-10], as the carriers must transit disordered regions. At low *T* when the phonon scattering is weak, the disordered regions become regions of localization so that $\Omega_p \rightarrow 0$ and σ_{DC} shows the strong *T* dependence of insulating samples [1,2]. The presence of negative magnetoresistance at low *T* is consistent with weak localization in some conduction paths. In contrast to the large λ for the delocalized carriers, the large majority of the carriers which do not contribute to the low

frequency transport have $\tau \sim 10^{-15}$ s leading to $\lambda \sim 5$ Å, shorter than the $\lambda \sim 40$ Å expected for confinement to the crystalline regions. This difference might be accounted for by averaging over ordered and disordered regions and chain orientations.

4. Conclusions

In summary, with improved processing, PAN-CSA and PPy-PF_6, model quasi-1D conductors, demonstrate metallic transport. At *RT*, a small fraction (10^{-3}) of carriers are delocalized with $\tau > 10^{-13}$ s, inconsistent with the Ioffe-Regel condition, while the majority of carriers are localized with $\tau \sim 10^{-15}$ s. Systems on the metallic side of the IMT are characterized by finite σ_{DC} and finite Ω_p as $T \to 0$. In contrast, systems on the insulating side of the IMT have a strongly T dependent σ_{DC} and $\Omega_p \to 0$ as $T \to 0$. A homogeneous Anderson transition is not appropriate for conducting polymers because (1) the T dependence of σ_{DC} does not monotonically weaken with increasing $\sigma_{DC}(RT)$; (2) the mK σ_{DC} shows a negative magnetoresistance and a T dependence inconsistent with variable range hopping for insulating samples; (3) $\Omega_p(T)$ scales with $\sigma_{DC}(T)$ and not the low T W plot; and (4) τ grows as T decreases. $\sigma_{DC}(T)$ and $\varepsilon(\omega,T)$ are consistent with the behavior of percolating composite systems. Thus, a percolating composite with inhomogeneous disorder is proposed, accounting for the quasi-1D localization and phonon-induced delocalization in disordered regions between fuzzy crystalline regions.

Acknowledgment

We thank V. N. Prigodin for useful discussions and R. Rochlin and T. Lemberger for experimental assistance. This work was supported by NIST ATP 1993-01-0149 and NSF DMR-9508723. D. T. acknowledges NSF DMR-9103894. G. I. acknowledges the University of Florida Division of Sponsored Research.

References

[1] A. J. Epstein, J. Joo, R. S. Kohlman, G. Du, E. J. Oh, Y. Min, J. Tsukamoto, H. Kaneko, and J. P. Pouget, Synth. Met. **65**, 149 (1994).

[2] R. S. Kohlman, J. Joo, and A. J. Epstein, in Physical Properties of Polymers Handbook, edited by J. E. Mark, (AIP Press, Woodbury, 1996), p. 435.

[3] T. Ishiguro, H. Kaneko, Y. Nogami, H. Ishimoto, H. Nishiyama, J. Tsukamoto, A. Takahashi, M. Yamaura, T. Hagiwara, and K. Sato, Phys. Rev. Lett. **69**, 660 (1992); Y. Nogami, H. Kaneto, H. Ito, T. Ishiguro, T. Sasaki, N. Toyota, A. Takahashi, and J. Tsukamoto, Phys. Rev. B **43**, 11829 (1991).

[4] R. S. Kohlman, A. Zibold, D. B. Tanner, G. G. Ihas, Y. G. Min, A. G. MacDiarmid, and A. J. Epstein, to be published.

[5] J. C. Clark, G. G. Ihas, A. F. Rafanello, M. W. Meisel, M. Reghu, C. O. Yoon, Y. Cao, and A. J. Heeger, Synth. Met. 69, 215 (1995).

[6] F. Zuo, M. Angelopoulos, A. G. MacDiarmid, and A. J. Epstein, Phys. Rev. B. **36**, 3475 (1987).

[7] J. Joo, Z. Oblakowski, G. Du, J. P. Pouget, E. J. Oh, J. M. Weisinger, Y. G. Min, A. G. MacDiarmid, and A. J. Epstein, Phys. Rev. B **49**, 2977 (1994).

[8] J. Joo, V. N. Prigodin, Y. G. Min, A. G. MacDiarmid, and A. J. Epstein, Phys. Rev. B **50**, 12226 (1994).

[9] R. S. Kohlman, J. Joo, Y. Z. Wang, J. P. Pouget, H. Kaneko, T. Ishiguro, and A. J. Epstein, Phys. Rev. Lett. **74**, 773 (1995).

[10] R. S. Kohlman, J. Joo, Y. G. Min, A. G. MacDiarmid, and A. J. Epstein, Phys. Rev. Lett. **77**, 2766 (1996).

[11] R. Pelster, G. Nimtz, and B. Wessling, Phys. Rev. B **49**, 12718 (1994).

[12] Reghu M., C. O. Yoon, D. Moses, A. J. Heeger, and Y. Cao, Phys. Rev. B **48**, 17685 (1993); Reghu M., Y. Cao, D. Moses, and A. J. Heeger, Phys. Rev. B **47**, 1758 (1993).

[13] K. Lee, A. J. Heeger, and Y. Cao, Phys. Rev. B **48**, 14884 (1993).

[14] N. F. Mott and E. Davis, Electronic Processes in Non-Crystalline Materials (Clarendon Press, Oxford, 1979).

[15] N. F. Mott and M. Kaveh, Adv. in Phys. **34**, 329 (1985).

[16] P. A. Lee and T. V. Ramakrishnan, Rev. Mod. Phys. **57**, 287 (1985).

[17] P. W. Anderson, Phys. Rev. **109**, 1492 (1958); ibid, Comments Solid State Phys. **2**, 193 (1970).

[18] V. N. Prigodin, private communications.

[19] A. G. Zabrodskii and K. N. Zeninova, Zh. Eskp. Teor. Fiz. **86**, 727 (1984) [Sov. Phys. JETP **59**, 425 (1984)].

[20] A. F. Ioffe and A. R. Regel, Prog. Semicond. **4**, 237 (1960).

[21] F. Wooten, Optical Properties of Solids (Academic, New York, 1972).

[22] J. P. Pouget, Z. Oblakowski, Y. Nogami, P. A. Albouy, M. Laridjani, E. J. Oh, Y. Min, A. G. MacDiarmid, J. Tsukamoto, T. Ishiguro, and A. J. Epstein, Synth. Met. **65**, 131 (1994).

[23] A. G. MacDiarmid and A. J. Epstein, Synth. Met. **65**, 103 (1994); A. G. MacDiarmid and A. J. Epstein, Proc. 2nd Braz. Polym. Conf., 5-8 Oct. 1993 (Plenum Pub. Corp.) p. 554.

[24] R. P. McCall, E. M. Scherr, A. G. MacDiarmid, and A. J. Epstein, Phys. Rev. B **50**, 5094 (1994).

[25] V. N. Prigodin and K. B. Efetov, Phys. Rev. Lett. **70**, 2933 (1993).

[26] D. J. Bergman and D. Stroud, in Solid State Physics **46**, edited by H. Ehrenreich and D. Turnbull (Academic Press, New York, 1992).

[27] Y. Cao and A. J. Heeger, Synth. Met. **52**, 193 (1992).

[28] B. Movaghar and S. Roth, Synth. Met. **63**, 163 (1993).

[29] T. Holstein, Ann. Phys. **8**, 325 (1959).

[30] H. H. S. Javadi, A. Chakraborty, C. Li, N. Theophilou, D. B. Swanson, A. G. MacDiarmid, and A. J. Epstein, Phys. Rev. B **43**, 2183 (1991).

[31] G. Leising, Phys. Rev. B **38**, 10313 (1988); J. Tanaka, S. Hasegawa, T. Miyamae, and M. Shimizu, Synth. Met. **41-43**, 1199 (1991); H. S. Woo, D. B. Tanner, , N. Theophilou, and A. G. MacDiarmid, Synth. Met. **41-43**, 159 (1991).

[32] S. Stafstrom, J. L. Bredas, A. J. Epstein, H. S. Woo, D. B. Tanner, W. S. Huang, and A. G. MacDiarmid, Phys. Rev. Lett. **59**, 1464 (1987).